

Space Processor Computation Time Analysis for Reinforcement Learning and Run Time Assurance Control Policies

Kyle Dunlap^{*1} and Nathaniel Hamilton^{†1}
Parallax Advanced Research, Beavercreek, OH, 45431, USA

Francisco Viramontes[‡]
COSMIAC, Albuquerque, NM, 87106, USA

Derrek Landauer[§]
BlueHalo, Albuquerque, NM, 87123, USA

Evan Kain[¶]
Air Force Research Laboratory, Kirtland Air Force Base, NM, 87117, USA

Kerianne L. Hobbs^{||}
Air Force Research Laboratory, Wright-Patterson Air Force Base, OH, 45433, USA

As the number of spacecraft on orbit continues to grow, it is challenging for human operators to constantly monitor and plan for all missions. Autonomous control methods such as reinforcement learning (RL) have the power to solve complex tasks while reducing the need for constant operator intervention. By combining RL solutions with run time assurance (RTA), safety of these systems can be assured in real time. However, in order to use these algorithms on board a spacecraft, they must be able to run in real time on space grade processors, which are typically outdated and less capable than state-of-the-art equipment. In this paper, multiple RL-trained neural network controllers (NNCs) and RTA algorithms were tested on commercial-off-the-shelf (COTS) and radiation tolerant processors. The results show that all NNCs and most RTA algorithms can compute optimal and safe actions in well under 1 second with room for further optimization before deploying in the real world.

I. Introduction

FOR *On-orbit Servicing, Assembly, and Manufacturing* (OSAM) missions, docking and inspection tasks enable spacecraft operators to assess, plan for, and execute a wide variety of objectives. While these tasks are traditionally executed using classical control methods, this requires constant monitoring and adjustment by human operators, which becomes challenging or even impossible as the number of spacecraft increases. Therefore, the growing number of space assets and increasing complexity of operations makes the development of autonomous spacecraft operation critically important.

One promising solution for this problem is to utilize *Deep Reinforcement Learning* (RL) to learn optimal control policies, in the form of Neural Network Controllers (NNCs), for executing tasks in increasingly complex scenarios. RL is a fast-growing field for developing high-performing autonomy with growing impact spurred by success in agents that learn to beat human experts in games like Go [1], Starcraft [2], and Gran Turismo [3]. RL has also demonstrated success reacting in real-time to changing mission objectives and environment uncertainty, which is crucial for spacecraft operations [4, 5]. Additionally, RL has already demonstrated success in the space domain for inspecting illuminated ([6]) and uncooperative ([7]) space objects as well as collision-free docking [4, 8–11].

^{*}AI Software Developer, Intelligent Systems Division, AIAA Professional Member.

[†]AI Scientist, Intelligent Systems Division.

[‡]Research Scholar.

[§]Senior Computer Engineer, Space Systems Research.

[¶]Principal Investigator for Space Computing, Space Electronics Technology (SET) Program.

^{||}Safe Autonomy Lead, Autonomy Capability Team (ACT3), AIAA Associate Fellow.

¹These authors contributed equally to this work.

Despite these successes using RL for complex, dynamic challenges, they are predominantly limited to virtual environments. RL agents trained in simulation to solve real-world problems can present unexpected and catastrophic behavior when deployed [12, 13]. This is caused when the system enters scenarios that differ from the examples seen in training that produce a suboptimal control output that drives the system further from known scenarios that could be dangerous. Efforts in Safe RL ([11, 14–23]) have helped reduce these catastrophic events, but without formally verifying NNCs, there is no guarantee it will not happen. Therefore, to use high-performing NNCs in the real world, they must be bound by Run Time Assurance (RTA).

RTA is an online safety assurance technique for ensuring the safe operation of control systems by filtering the output of the primary control (e.g. a NNC), intervening as necessary to assure system safety [24]. The RTA method focused on in this paper uses control barrier functions (CBFs) to assure safety, where an optimization algorithm is solved to obtain a safe control input as close as possible to the desired control input. Using CBFs allows RTA to enforce multiple safety constraints simultaneously.

However, fixing the safety concerns using RTA introduces a new concern: computation time. Because developing space-grade hardware is a costly and lengthy process, the hardware tends to be outdated and has far less capability than state-of-the-art hardware [25]. This has led to concerns about running NNCs and RTA fast enough to control a spacecraft in real-time since using CBFs to assure safety requires continually solving an optimization algorithm in real time, which is a computationally intense. This work seeks to assuage these concerns by measuring the execution times for NNCs and RTAs on a variety of space-grade hardware to identify expected timing requirements.

The main contribution focuses on providing timing results from running NNCs and RTAs on space-grade hardware. Additionally this work presents comparisons that could lead to future improvements that could result in faster execution times. This work builds on previous research to train an RL agent to complete an inspection problem [6], and developing RTA constraints for the same task [26]. The results from this work demonstrate that, even without further optimization, NNCs and RTA can produce a safe and optimal control value in under 20ms* on COTS and radiation tolerant processors.

II. Background

This section provides introductions to reinforcement learning, run time assurance, and the types of space grade hardware used in this work.

A. Reinforcement Learning

Reinforcement Learning is a form of machine learning in which an agent acts in an environment, learns through experience, and improves the performance of the learned behaviour function, i.e. policy, based on the observed reward. The environment can be comprised of any dynamical system, from Atari simulations ([14, 27]) to complex robotics scenarios ([12, 16, 28–31]).

In *Deep Reinforcement Learning* (RL) the policy is approximated using a deep neural network, which becomes the *Neural Network Controller* (NNC) after training is completed. This work focuses on NNCs trained using the Proximal Policy Optimization (PPO) algorithm. PPO was first introduced in [32]. The “proximal” in PPO refers to how the algorithm focuses on iteratively improving the policy in small increments to prevent against making large changes in the policy that lead to drops in performance. PPO was selected because of its widespread use in a variety of RL tasks and previous demonstrated success in the space domain [6, 8, 9, 11, 23].

B. Run Time Assurance

Run Time Assurance (RTA) is an online safety assurance technique that filters potentially unsafe inputs from a primary controller and intervenes as necessary to assure system safety [24]. The primary controller can come in many different forms, such as the NNC trained with RL, a classical control technique, or even a human operator. It is decoupled from the RTA filter, and can completely focus on completing the task while the RTA filter focuses on assuring safety. A feedback control system with RTA is shown in Fig. 1. The primary controller receives the state \mathbf{x} and computes a desired control input \mathbf{u}_{des} to pass to the RTA filter. The RTA filter evaluates \mathbf{u}_{des} based on the current state and modifies it as necessary to produce a safe control input \mathbf{u}_{act} to pass to the plant.

For a continuous time control affine dynamical system defined as,

$$\dot{\mathbf{x}} = f(\mathbf{x}) + g(\mathbf{x})\mathbf{u}, \quad (1)$$

*This is assuming the RTA is explicit, continuous ASIF.

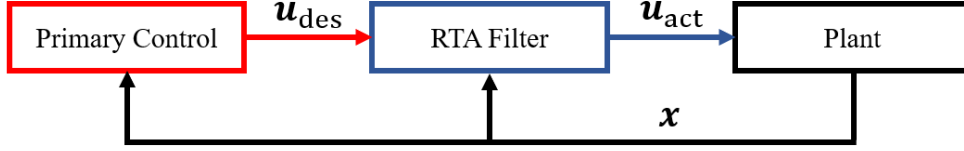


Fig. 1 Feedback control system with RTA filter. Components with low safety confidence are outlined in red, and components with high safety confidence are outlined in blue.

where $f : \mathcal{X} \rightarrow \mathbb{R}^n$ and $g : \mathcal{X} \rightarrow \mathbb{R}^{n \times m}$ are locally Lipschitz continuous functions. $\mathbf{x} \in \mathcal{X} \subseteq \mathbb{R}^n$ denotes the state vector, $\mathbf{u} \in \mathcal{U} \subseteq \mathbb{R}^m$ denotes the control vector, \mathcal{X} is the set of all possible state values, and \mathcal{U} is the admissible control set.

To define safety of this system at the current time, consider the superlevel set of a continuously differentiable function $\varphi : \mathcal{X} \rightarrow \mathbb{R}$ defined as $C_\varphi = \{\mathbf{x} \in \mathcal{X} : \varphi(\mathbf{x}) \geq 0\}$, where C_φ is referred to as the allowable set. The system will be safe for all time if it is in a forward invariant subset of C_φ known as the safe set $C_S \subseteq C_\varphi \subset \mathbb{R}^n$, where for every $\mathbf{x} \in C_S$, $\mathbf{x}(t) \in C_S, \forall t \geq 0$. A continuously differentiable function $h : \mathcal{X} \rightarrow \mathbb{R}$ is used to define C_S , where $C_S = \{\mathbf{x} \in \mathcal{X} : h(\mathbf{x}) \geq 0\}$. To enforce forward invariance of C_S , Nagumo's condition [33] is used, where the boundary of C_S is examined to ensure $\dot{h}(\mathbf{x}) \geq 0$. To relax this condition away from the boundary, a continuous function $\alpha : \mathbb{R} \rightarrow \mathbb{R}$ is introduced, where α is an extended class \mathcal{K} function that is strictly increasing and has the property $\alpha(0) = 0$. Safety can be enforced using Control Barrier Functions (CBFs) [34], where h is a CBF if there exists an extended class \mathcal{K} function α and control $\mathbf{u} \in \mathcal{U}$ such that,

$$\sup_{\mathbf{u} \in \mathcal{U}} [L_f h(\mathbf{x}) + L_g h(\mathbf{x})\mathbf{u}] \geq -\alpha(h(\mathbf{x})), \forall \mathbf{x} \in C_S, \quad (2)$$

where L_f and L_g are Lie derivatives of h along f and g respectively.

To enforce safety inside the control loop, this paper uses the RTA technique known as the Active Set Invariance Filter (ASIF) [35]. ASIF is a first-order optimization algorithm that is minimally invasive towards the primary controller. It is formulated as a Quadratic Program (QP), where the objective function is the l^2 norm difference between \mathbf{u}_{des} and \mathbf{u}_{act} . CBFs are defined as inequality constraints, known as barrier constraints, and are used to enforce safety where,

$$BC(\mathbf{x}, \mathbf{u}) := L_f h(\mathbf{x}) + L_g h(\mathbf{x})\mathbf{u} + \alpha(h(\mathbf{x})) \geq 0. \quad (3)$$

For N barrier constraints, the ASIF algorithm is defined as,

Active Set Invariance Filter

$$\begin{aligned} \mathbf{u}_{\text{act}}(\mathbf{x}, \mathbf{u}_{\text{des}}) &= \underset{\mathbf{u} \in \mathcal{U}}{\text{argmin}} \|\mathbf{u}_{\text{des}} - \mathbf{u}\| \\ \text{s.t. } BC(\mathbf{x}, \mathbf{u}) &\geq 0, \forall i \in \{1, \dots, N\} \end{aligned} \quad (4)$$

For the dynamical system in (1), the barrier constraints can be defined explicitly as,

$$BC_i(\mathbf{x}, \mathbf{u}) := \nabla h_i(\mathbf{x})(f(\mathbf{x}) + g(\mathbf{x})\mathbf{u}) + \alpha_i(h_i(\mathbf{x})). \quad (5)$$

In this case, safety is defined offline to ensure the CBFs render C_S forward invariant. This RTA technique will be referred to as explicit ASIF (eASIF).

Safety can also be defined implicitly online, where closed loop trajectories under a predetermined backup control law \mathbf{u}_b are continuously computed to ensure C_S can be rendered forward invariant. In this case, the barrier constraint is based on C_φ , and is defined implicitly as,

$$BC_i(\mathbf{x}, \mathbf{u}) := \nabla \varphi_i(\phi_j^{\mathbf{u}_b}) D(\phi_j^{\mathbf{u}_b}) [f(\mathbf{x}) + g(\mathbf{x})\mathbf{u}] + \alpha_i(\varphi_i(\phi_j^{\mathbf{u}_b})), \quad (6)$$

where $\phi_j^{\mathbf{u}_b}$ defines a prediction of the state \mathbf{x} at the j^{th} discrete time interval $\forall t \in [0, \infty)$ along the trajectory computed under \mathbf{u}_b , and $D(\phi_j^{\mathbf{u}_b})$ is computed by integrating a sensitivity matrix along this trajectory [36]. This RTA technique will be referred to as implicit ASIF (iASIF). Note that for practical implementation, the trajectories are limited to a finite time horizon T .

Finally, safety can also be computed in discrete time, which can be useful when the RTA filter must be run at a lower frequency. For a discrete time dynamical system defined as,

$$\mathbf{x}_{t+\Delta t} = f(\mathbf{x}_t, \mathbf{u}_t), \quad (7)$$

a continuously differentiable function $h : \mathcal{X} \rightarrow \mathbb{R}$ is a discrete CBF (DCBF) [37] if there exists an extended class \mathcal{K} function α satisfying $\alpha(r) < r, \forall r > 0$, and $\mathbf{u} \in \mathcal{U}$ such that,

$$\Delta h(\mathbf{x}_t, \mathbf{u}_t) + \alpha(h(\mathbf{x}_t)) \geq 0, \quad \forall \mathbf{x}_t \in C_S, \quad (8)$$

where,

$$\Delta h(\mathbf{x}_t, \mathbf{u}_t) = \frac{h(\mathbf{x}_{t+\Delta t}) - h(\mathbf{x}_t)}{\Delta t}. \quad (9)$$

The discrete barrier constraint is therefore defined as,

$$BC_i(\mathbf{x}_t, \mathbf{u}_t) := \Delta h_i(\mathbf{x}_t, \mathbf{u}_t) + \alpha_i(h_i(\mathbf{x}_t)) \geq 0. \quad (10)$$

Notably, due to the computation of $\mathbf{x}_{t+\Delta t}$, these constraints often become nonlinear. Therefore, a nonlinear solver is used to solve the ASIF algorithm rather than a QP. In general, nonlinear solvers are incomplete and are much slower than QPs. This RTA technique will be referred to as discrete ASIF (dASIF).

C. Space Hardware

Due to radiation hazards that exist in space such as galactic cosmic rays, solar particle events, and trapped radiation in the Van Allen belts, processors on board spacecraft must be specially designed to withstand the space environment [25]. Without this, radiation can cause issues such as data corruption or a malfunction of the processor. However, because developing space grade hardware is often a costly and lengthy process, this hardware tends to be outdated and have far less capability than state of the art hardware. This makes it challenging to run modern control algorithms that are designed to be run in real time.

Space grade hardware can be divided into three main categories: *Commercial Off The Shelf* (COTS), radiation tolerant, and radiation hardened. COTS hardware is not specifically designed to withstand radiation, and as a result it is generally used for shorter term missions in *Low Earth Orbit* (LEO) and not for missions in *Geostationary Earth Orbit* (GEO). Radiation tolerant hardware is able to withstand some radiation, and is generally used for medium term missions in LEO or short term missions in GEO. Radiation hardened hardware can withstand a significant amount of radiation, and can be used for long term missions in LEO or GEO. While ideally all processors used in space would be radiation hardened, the designer must balance cost, availability, and functionality when choosing processors for their mission.

III. Experimental Setup

This section introduces the spacecraft inspection task, the NNC architecture and RTA constraints to be tested, the specific processors used for experimentation, and a description of all experimental configurations.

A. Inspection Task

In this work, the NNCs and RTA are designed for completing the inspection task introduced in [6]. The inspection task considers an active “deputy” spacecraft attempting to inspect a passive “chief” spacecraft [6]. The analysis takes place in Hill’s frame [38], shown in Fig. 2, where the chief is in a circular orbit around the Earth, and the agent controls the deputy. The chief is represented by a sphere of 99 uniformly distributed points, where points can only be inspected if they are within the deputy’s field of view and are illuminated by the Sun.

1. Dynamics

The dynamics for the inspection task are modeled using the Clohessy-Wiltshire equations [39] in Hill’s frame, where the origin O_H is located at the chief’s center of mass, the unit vector \hat{x} points away from the center of the Earth, \hat{y} points in the direction of motion of the chief, and \hat{z} is normal to \hat{x} and \hat{y} . The linearized relative motion dynamics between the deputy and chief are defined as,

$$\dot{\mathbf{x}} = \mathbf{A}\mathbf{x} + \mathbf{B}\mathbf{u}, \quad (11)$$

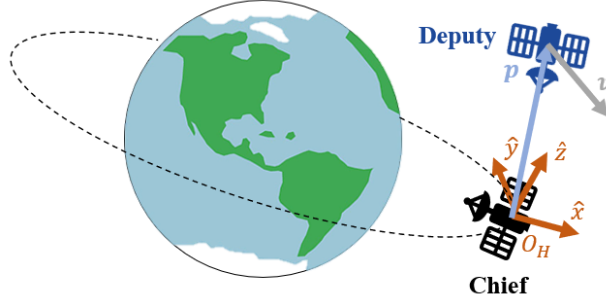


Fig. 2 Deputy spacecraft in relation to a chief spacecraft in Hill's Frame.

where \mathbf{x} is the state vector $\mathbf{x} = [x, y, z, \dot{x}, \dot{y}, \dot{z}]^T \in \mathbb{R}^6$, \mathbf{u} is the control vector, $\mathbf{u} = [F_x, F_y, F_z]^T \in [-\mathbf{u}_{\max}, \mathbf{u}_{\max}]^3$, and,

$$A = \begin{bmatrix} 0 & 0 & 0 & 1 & 0 & 0 \\ 0 & 0 & 0 & 0 & 1 & 0 \\ 0 & 0 & 0 & 0 & 0 & 1 \\ 3\eta^2 & 0 & 0 & 0 & 2\eta & 0 \\ 0 & 0 & 0 & -2\eta & 0 & 0 \\ 0 & 0 & -\eta^2 & 0 & 0 & 0 \end{bmatrix}, B = \begin{bmatrix} 0 & 0 & 0 \\ 0 & 0 & 0 \\ 0 & 0 & 0 \\ \frac{1}{m} & 0 & 0 \\ 0 & \frac{1}{m} & 0 \\ 0 & 0 & \frac{1}{m} \end{bmatrix}. \quad (12)$$

Here, $\eta = 0.001027\text{rad/s}$ is the mean motion of the chief's orbit, $m = 12\text{kg}$ is the mass of the deputy, F is the force exerted by the deputy's thrusters along each axis, and $\mathbf{u}_{\max} = 1\text{N}$ is the maximum force. The attitude of the deputy is not modeled, and it is assumed that it is always pointing towards the chief.

The Sun is assumed to remain in a constant position in relation to the Earth, where it appears to rotate in Hill's frame. For this task, the Sun rotates in the $\hat{x} - \hat{y}$ plane in Hill's frame, where the unit vector pointing from the center of the chief spacecraft to the Sun, \hat{r}_S , is defined as,

$$\hat{r}_S = [\cos \theta_{\text{Sun}}, \sin \theta_{\text{Sun}}, 0], \quad (13)$$

where $\dot{\theta}_{\text{Sun}} = -\eta$. It is also assumed that nothing blocks the chief from being illuminated.

2. RL Environment Setup

The RL environment is partially observable, where sensors are used to consolidate full state information into components of the observation space. In addition to the state $[x, y, z, \dot{x}, \dot{y}, \dot{z}]$ and sun angle θ_{Sun} as defined above, the agent receives two additional observations related to the inspection points: the total number of points that have been inspected during the episode n_p , and a unit vector pointing towards the nearest cluster of uninspected points $\hat{r}_{UPS} = [x_{UPS}, y_{UPS}, z_{UPS}]$, as determined by k-means clustering. Two observation spaces are considered for this analysis, where the first is referred to as "no sensors" and is defined as,

$$\mathbf{o}_{\text{no}} = [x, y, z, \dot{x}, \dot{y}, \dot{z}]. \quad (14)$$

The second observation space is referred to as "all sensors" and is defined as,

$$\mathbf{o}_{\text{all}} = [x, y, z, \dot{x}, \dot{y}, \dot{z}, n_p, \theta_{\text{Sun}}, x_{UPS}, y_{UPS}, z_{UPS}]. \quad (15)$$

3. Safety Constraints

While many safety constraints could be developed for the inspection task, the following constraints are enforced for this analysis. First, the deputy shall not collide with the chief. The CBF for this constraint is defined as,

$$h_1(\mathbf{x}) := \sqrt{2a_{\max} [\|\mathbf{p}\|_2 - (d_d + d_c)]} + v_{prc} \geq 0, \quad (16)$$

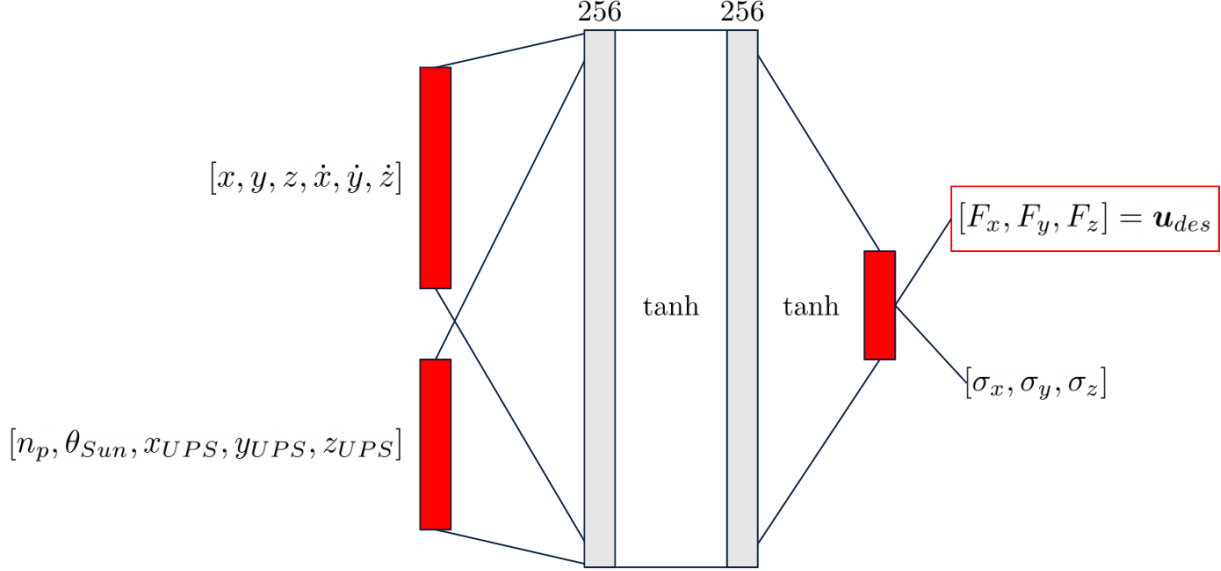


Fig. 3 The NNC architecture for the “all sensors” variation of the inspection task.

where a_{\max} is the maximum acceleration of the deputy, \mathbf{p} is the deputy’s position, d_d and d_c are the collision radii of the deputy and chief respectively, and \mathbf{v}_{prc} is the projection of the deputy’s velocity in the direction of the chief. This constraint ensures that the deputy can slow down to avoid a collision.

Second, the deputy shall remain in proximity with the chief so that it stays on task. This is treated as a keep in zone, and the CBF for this constraint is defined as,

$$h_2(\mathbf{x}) := \sqrt{2a_{\max}(d_{\max} - \|\mathbf{p}\|_2)} - \mathbf{v}_{prc} \geq 0, \quad (17)$$

where d_{\max} is the maximum relative distance from the chief, and in this case \mathbf{v}_{prc} is the projection of the deputy’s velocity in the direction of the keep in zone.

Third, the deputy shall slow down as it approaches the chief, which reduces the risk of a potential collision in the event of a fault. The CBF for this constraint is defined as,

$$h_3(\mathbf{x}) := v_0 + v_1 \|\mathbf{p}\|_2 - \|\mathbf{v}\|_2 \geq 0, \quad (18)$$

where v_0 is a minimum allowable speed at the origin, v_1 is a constant rate at which \mathbf{p} shall decrease, and \mathbf{v} is the deputy’s velocity.

Finally, the deputy shall not maneuver aggressively with high velocities. This is defined as three separate CBFs,

$$h_4(\mathbf{x}) := v_{\max}^2 - \dot{x}^2 \geq 0, \quad h_5(\mathbf{x}) := v_{\max}^2 - \dot{y}^2 \geq 0, \quad h_6(\mathbf{x}) := v_{\max}^2 - \dot{z}^2 \geq 0, \quad (19)$$

where v_{\max} is the maximum allowable velocity. Further details for all constraints can be found in [26].

The safe set is then defined as $C_S = \{\mathbf{x} \in \mathcal{X} : h_i(\mathbf{x}) \geq 0, \forall i \in \{1, \dots, 6\}\}$. The CBFs are enforced simultaneously by the ASIF algorithm. For simplicity and equal comparison, the same CBFs are used for explicit, implicit, and discrete ASIF.

B. Neural Network Controllers

This work focuses on testing two NNCs trained to solve the two variations of the inspection task described in Section III.A.2. The hyperparameters used to train the NNCs using the PPO algorithm for these experiments are listed in Table 1. The NNC architecture for the “all sensors” variation is shown in Fig. 3. The “no sensors” variation has the same architecture, but with the bottom input block removed.

The NNC architecture is a fully-connected Multi-Layer Perceptron (MLP) network with two hidden layers with 256 nodes each. The hidden layers have a tanh activation function[†]. The NNC has either 6 inputs or 11 inputs, depending

[†]This is the common/default architecture used for PPO.

on the observation space used. The output layer consists of 6 nodes, which represent the mean and variance for each control value in \mathbf{u} for a stochastic policy used during training. In these experiments, the output is always the mean value as show by the red box in Fig. 3. The inputs are normalized such that typical values fall within the range $[-1, 1]$, where $[x, y, z]$ are each divided by 100, $[\dot{x}, \dot{y}, \dot{z}]$ are each multiplied by 2, and n_p is divided by 100. Further details of the RL environment and training process can be found in [6].

Table 1 PPO Training Hyperparameters

Parameter	Value
Number of SGD iterations	30
Discount factor γ	0.99
GAE- λ	0.928544
Max episode length	1223
Rollout fragment length	1500
Train batch size	1500
SGD minibatch size	1500
Total timesteps	5×10^6
Learning rate	5×10^{-5}
KL initial coefficient	0.2
KL target value	0.01
Value function loss coefficient	1.0
Entropy coefficient	0.0
Clip parameter	0.3
Value function clip parameter	10.0

C. Space Processors

The processors used for testing are listed in Table 2, which were provided by the Spacecraft Processing Architectures and Computing Environment Research (SPACER) laboratory. For this analysis, three COTS processors and one radiation tolerant processor were tested. For all tests, only the CPU was used to estimate worst case performance in the real world. Additionally, all tests recorded the time from receiving the inputs to publishing the output.

Table 2 Processor Specifications

Board	Radiation	Cores	CPU Max Frequency	Memory Speed	Power	GPU/FPGA
Jetson AGX Orin	COTS	12	2.2 GHz	204.8 GB/s	15 - 60 W	✓/ X
Jetson Orin Nano	COTS	6	1.5 GHz	68 GB/s	7 - 15 W	✓/ X
Jetson AGX Xavier	COTS	8	2.2 GHz	136.5 GB/s	10 - 30 W	✓/ X
Unibap iX10	Rad-Tolerant	4	3.6 GHz	2.34 GB/s	<40 W	✓/ ✓

1. COTS

For all tests on the COTS processors, Python was used to run the NNC and RTA. The NNCs were trained using the Air Force Research Laboratory’s Core Reinforcement Learning library (CoRL) [40] and the RTA was originally developed in the Safe Autonomy Run Time Assurance Framework [41], which are both written in Python and allowed for a simple transition to the processors. After training the NNCs, ONNX Runtime [42] was used to convert them into simple models that could be run on the processors. For the RTA, Quadprog [43] was used for the ASIF QP, and SciPy’s SLSQP algorithm [44] was used as the nonlinear solver for dASIF. NumPy [45] was used for all linear algebra. ROS2

[46] was used to run the algorithms on the processors, which represents a realistic framework for passing messages in data in a similar manner to what would be used on board a spacecraft.

2. Radiation Tolerant

For all tests on the Unibap iX10, C++ was used to run the NNC and RTA. While it may have been possible to run Python on this processor, C and C++ are much more commonly used on space grade hardware. Therefore, an effort was made to ensure the algorithms tested were of this format. ONNX Runtime was used to run the NNC. For the RTA, QuadProg++ [47] was used for the QP, and the NLOpt COBYLA algorithm [48] was used as the nonlinear solver. Eigen [49] was used for linear algebra. For these tests, simple scripts were made to pass data and record the computation time.

D. Experiments

Many different configurations were tested on the COTS and radiation tolerant processors. At a high level, these configurations can be divided into three groups: NNC only, RTA only, and NNC combined with RTA. Each configuration was tested with 1,000 test cases, each corresponding to a different state. These states were divided into two groups: “safe” states that are guaranteed to be within C_S , and “not safe” states that may or may not be in C_S . For the configurations that include an NNC, the NNC with all sensors (as defined in Section III.A.2) was tested on the COTS processors, and NNCs with either no sensors or all sensors were tested on the iX10. For the RTA only configurations, a set of 1,000 random actions were used to represent the primary controller.

For all RTA configurations, each different RTA filter was considered. First, eASIF was tested, which represents the baseline configuration. Next, iASIF was tested with two different timesteps for the computed backup trajectory: 1 s and 10 s. The total trajectory length $T = 20$ s in each case, so this results in either 20 or 2 computed trajectory steps. Finally, dASIF was also tested with the same two timesteps, which in this case correspond to when the next state is computed. For only the tests on the iX10, two different tolerances were also considered: $1e-3$ and $1e-4$. These tolerances are the relative and absolute tolerances of the optimization algorithm, and they control how accurate the solution is which directly affects computation time.

For benchmarking purposes, the execution time for each test case was recorded. The main metric presented is the *InterQuartile Mean* (IQM) of the execution time, which discards the highest and lowest 25% of the recorded data and calculates the mean score on the remaining middle 50% of data. The IQM is more robust to outliers, and is a better representation of the expected execution time [50]. The worst case execution time is also of interest, but it is often unknown or difficult to derive [51]. Therefore, the *Maximal Observed Execution Time* (MOET) is presented instead. Additional metrics are provided in Section IV for completeness. Also note that ONNX Runtime uses Just In Time (JIT) compilation, meaning the model is compiled during the first time it is run. This time is separated into a separate column for Table 6 and Table 8.

IV. Results

This section provides all the timing results collected from the COTS and radiation tolerant hardware. A discussion of trends found in selected results are presented in Section V.

A. COTS Timing Results

The full timing results from running the experiments on COTS hardware are shown in the following tables. These results come from measuring the execution time for 1,000 test cases for each row. Table 3 shows the timing result executing only the NNC on all COTS processors. Table 4 shows the timing result executing only the RTA filtering randomly selected actions on all COTS processors. Table 5 shows the timing result executing the NNC and RTA in series on all COTS processors.

Table 3 Neural Network Controller only (all sensors) for COTS processors (ms)

Metric Labels	IQM	Mean	St. Dev.	Min	Median	Max
AGX Orin (safe)	1.187445	1.228211	0.609142	0.234604	1.152396	2.985716
AGX Orin (not safe)	1.274283	1.251544	0.544837	0.260115	1.270294	3.172636
AGX Xavier (safe)	0.955370	0.987614	0.116162	0.778198	0.937819	1.774073
AGX Xavier (not safe)	0.943299	0.985999	0.218077	0.553131	0.849485	2.014160
Orin Nano (safe)	0.826063	0.832814	0.116105	0.621319	0.826120	3.330231
Orin Nano (not safe)	0.816813	0.821106	0.156956	0.595808	0.817776	5.327463

Table 4 Run Time Assurance only for COTS processors (ms)

Metric Labels	IQM	Mean	St. Dev.	Min	Median	Max
AGX Orin eASIF (safe)	2.750907	3.329385	1.815636	1.415491	2.644897	13.191223
AGX Orin eASIF (not safe)	3.828257	4.387763	2.386426	1.437187	3.249407	14.296770
AGX Orin dASIF dt=1 (safe)	16.464000	17.857730	7.505805	6.291151	16.286969	47.605753
AGX Orin dASIF dt=1 (not safe)	13.954637	15.005995	6.395238	6.036758	13.627291	42.531967
AGX Orin dASIF dt=10 (safe)	21.848526	21.802646	7.986108	6.202459	22.051692	50.238371
AGX Orin dASIF dt=10 (not safe)	23.385702	23.700129	15.179291	5.964756	24.177551	271.273613
AGX Orin iASIF dt=1 (safe)	12.569212	12.836350	2.253597	8.590221	12.634397	27.595997
AGX Orin iASIF dt=1 (not safe)	12.351090	12.849332	2.830778	8.388996	12.449384	26.875496
AGX Orin iASIF dt=10 (safe)	6.106794	6.150317	2.833092	1.900911	6.414652	19.070864
AGX Orin iASIF dt=10 (not safe)	8.107551	8.085205	2.096096	1.858711	8.245826	16.801119
AGX Xavier eASIF (safe)	6.780652	6.782235	1.046182	4.975796	6.831884	10.135412
AGX Xavier eASIF (not safe)	6.897135	6.911544	1.385440	4.483938	6.967545	37.313461
AGX Xavier dASIF dt=1 (safe)	21.084351	22.639788	8.528005	13.042927	22.226334	59.758186
AGX Xavier dASIF dt=1 (not safe)	22.660113	24.019467	9.195153	13.480902	22.806048	66.515207
AGX Xavier dASIF dt=10 (safe)	36.319591	33.975447	10.832311	13.076067	39.674759	99.483728
AGX Xavier dASIF dt=10 (not safe)	35.776018	35.831206	30.146673	13.020277	38.898706	578.676701
AGX Xavier iASIF dt=1 (safe)	21.970631	21.874224	1.098860	19.713163	21.958470	26.401520
AGX Xavier iASIF dt=1 (not safe)	20.737039	21.076036	1.191656	19.755125	20.685315	38.733482
AGX Xavier iASIF dt=10 (safe)	8.145295	8.161349	0.850160	6.367683	8.159876	10.876656
AGX Xavier iASIF dt=10 (not safe)	35.422599	35.237457	27.231706	12.780905	38.780451	542.731047
Orin Nano eASIF (safe)	4.355317	4.319885	0.285863	2.608538	4.352689	4.872799
Orin Nano eASIF (not safe)	4.369097	4.489313	4.801894	2.299070	4.402399	147.660494
Orin Nano dASIF dt=1 (safe)	15.896380	17.493387	8.630736	9.178877	16.353846	173.128605
Orin Nano dASIF dt=1 (not safe)	17.178587	18.459619	7.733927	9.151459	17.144203	56.777000
Orin Nano dASIF dt=10 (safe)	24.952983	23.636972	9.078023	9.112358	27.179956	173.389673
Orin Nano dASIF dt=10 (not safe)	24.828254	24.594033	17.942731	9.175301	27.089834	366.775274
Orin Nano iASIF dt=1 (safe)	17.348053	17.301687	1.035882	12.364388	17.362356	24.291277
Orin Nano iASIF dt=1 (not safe)	17.102747	17.426064	2.161709	12.775660	17.038345	63.579559
Orin Nano iASIF dt=10 (safe)	5.636376	5.587431	0.376810	3.245831	5.637646	6.979465
Orin Nano iASIF dt=10 (not safe)	5.691443	5.645815	0.359121	3.118992	5.692244	7.040024

Table 5 Neural Network Controller (all sensors) and Run Time Assurance for COTS processors (ms)

Metric Labels	IQM	Mean	St. Dev.	Min	Median	Max
AGX Orin eASIF (safe)	2.416291	2.554553	1.128687	1.048565	2.466440	8.322716
AGX Orin eASIF (not safe)	4.610065	4.461648	1.998004	1.109600	5.039692	15.039921
AGX Orin dASIF dt=1 (safe)	9.103857	9.555218	2.373391	5.664825	9.035110	26.257515
AGX Orin dASIF dt=1 (not safe)	12.852021	13.881633	5.468681	5.748987	12.873411	44.796944
AGX Orin dASIF dt=10 (safe)	9.476149	9.678036	1.897095	5.804539	9.476662	16.189337
AGX Orin dASIF dt=10 (not safe)	10.646212	13.780409	30.656480	5.413771	10.231495	886.292696
AGX Orin iASIF dt=1 (safe)	13.380730	13.704895	3.052360	8.404255	13.133049	28.942347
AGX Orin iASIF dt=1 (not safe)	13.348919	13.793151	3.104095	8.520126	13.067245	31.623125
AGX Orin iASIF dt=10 (safe)	3.296854	3.630646	1.704423	1.539707	3.324151	13.426065
AGX Orin iASIF dt=10 (not safe)	5.201894	5.252436	2.341010	1.563787	5.368471	20.745516
AGX Xavier eASIF (safe)	4.372336	4.395119	0.579755	2.779245	4.352331	6.491184
AGX Xavier eASIF (not safe)	4.515870	4.493873	0.653715	2.696514	4.544854	6.919384
AGX Xavier dASIF dt=1 (safe)	15.325570	15.647139	2.177019	12.193918	15.392542	26.516199
AGX Xavier dASIF dt=1 (not safe)	14.981482	16.886219	5.844275	12.039185	15.101910	49.370050
AGX Xavier dASIF dt=10 (safe)	14.652752	15.066409	2.398740	11.744261	14.610052	28.725147
AGX Xavier dASIF dt=10 (not safe)	14.623624	20.185279	65.600733	11.199236	14.662147	1925.134420
AGX Xavier iASIF dt=1 (safe)	20.191029	20.298672	1.923566	18.255949	20.744324	45.238972
AGX Xavier iASIF dt=1 (not safe)	19.351970	19.717433	1.221049	18.252373	19.337416	25.688648
AGX Xavier iASIF dt=10 (safe)	5.933733	5.912681	0.761662	4.300117	5.967855	8.225441
AGX Xavier iASIF dt=10 (not safe)	6.097788	6.139364	0.554479	3.811359	6.030202	8.520126

B. Radiation Tolerant Timing Results

The full timing results from running the experiments on radiation tolerant hardware are shown in the following tables. These results come from measuring the execution time for 10,000 test cases for each row. Table 6 shows the timing result executing only the NNC on the radiation tolerant processor. Table 7 shows the timing result executing only the RTA filtering randomly selected actions on the radiation tolerant processor. Table 8 shows the timing result executing the NNC and RTA in series on the radiation tolerant processor.

Table 6 Neural Network Controller only for Unibap IX10 (ms)

Metric Labels	IQM	Mean	St. Dev.	Min	Median	Max	Execution with JIT
all sensors (safe)	0.024680	0.025994	0.004672	0.021951	0.024636	0.114974	0.790562
all sensors (not safe)	0.025528	0.026237	0.003622	0.022622	0.024786	0.156452	0.120034
no sensors (safe)	0.023983	0.025586	0.004621	0.022382	0.023504	0.080120	0.358081
no sensors (not safe)	0.024736	0.025361	0.003284	0.021911	0.024566	0.113533	0.316112

Table 7 Run Time Assurance only for Unibap IX10 (ms)

Metric Labels	IQM	Mean	St. Dev.	Min	Median	Max
eASIF (safe)	0.117673	0.123958	0.018850	0.107168	0.117154	0.403735
eASIF (not safe)	0.118868	0.122073	0.013497	0.107031	0.113589	0.421892
dASIF dt=1 tol=1e-3 (safe)	4.214526	38.633448	584.449966	0.829635	3.944832	17361.761425
dASIF dt=1 tol=1e-3 (not safe)	3.851534	11.168847	62.547584	0.793099	3.655996	1524.341135
dASIF dt=10 tol=1e-3 (safe)	8.827194	317.120068	3624.942297	0.798718	8.441662	60000.189866
dASIF dt=10 tol=1e-3 (not safe)	7.919051	54.155606	332.602006	0.836692	7.557296	7233.064712
dASIF dt=1 tol=1e-4 (safe)	9.419962	154.741459	1872.711906	4.278250	9.677567	47860.026079
dASIF dt=1 tol=1e-4 (not safe)	8.010065	55.016445	477.519387	4.194320	8.135115	9989.882471
dASIF dt=10 tol=1e-4 (safe)	14.932394	448.032044	4123.310098	4.202426	13.971648	60000.149681
dASIF dt=10 tol=1e-4 (not safe)	12.901447	371.274909	3696.299910	4.190733	12.136475	60000.098485
iASIF dt=1 (safe)	5.596083	5.573943	0.600580	4.672187	5.607997	8.721112
iASIF dt=1 (not safe)	5.421894	5.439027	0.609651	4.637850	5.294439	9.210239
iASIF dt=10 (safe)	0.546723	0.554855	0.062099	0.478004	0.513545	0.788635
iASIF dt=10 (not safe)	0.494691	0.505387	0.039198	0.471982	0.494978	0.806314

Table 8 Neural Network Controller and Run Time Assurance for Unibap IX10 (ms)

Metric Labels	IQM	Mean	St. Dev.	Min	Median	Max	Execution with JIT
eASIF all sensors (safe)	0.144337	0.148043	0.021234	0.140416	0.144263	1.998211	0.320026
eASIF all sensors (not safe)	0.145421	0.152326	0.016319	0.140015	0.144403	0.283246	0.284448
eASIF no sensors (safe)	0.148515	0.155292	0.018306	0.139888	0.148204	0.356702	0.347584
eASIF no sensors (not safe)	0.148306	0.153700	0.016972	0.139216	0.148113	0.395676	0.320242
dASIF dt=1 tol=1e-3 all sensors (safe)	3.721660	4.058949	1.240831	1.409485	3.714212	11.769172	6.820636
dASIF dt=1 tol=1e-3 all sensors (not safe)	3.708151	4.061183	1.271563	1.151727	3.625291	11.576846	5.041455
dASIF dt=1 tol=1e-3 no sensors (safe)	3.820180	11.449278	70.853788	0.854356	3.786309	1263.299591	3.359823
dASIF dt=1 tol=1e-3 no sensors (not safe)	3.938696	44.312923	1100.413853	0.850408	3.806449	34762.922707	2.928989
dASIF dt=10 tol=1e-3 all sensors (safe)	4.120237	4.509934	1.530665	1.434351	3.950538	13.016087	9.242374
dASIF dt=10 tol=1e-3 all sensors (not safe)	4.203840	4.570982	1.591459	1.429740	4.030370	30.398838	9.479227
dASIF dt=10 tol=1e-3 no sensors (safe)	7.107587	68.480251	951.044295	0.876166	6.877964	28919.426470	3.655862
dASIF dt=10 tol=1e-3 no sensors (not safe)	6.722149	47.481896	422.050374	0.867370	6.573830	10118.682149	4.680501
dASIF dt=1 tol=1e-4 all sensors (safe)	6.075389	6.691481	1.847697	4.435233	5.986329	16.914064	12.874864
dASIF dt=1 tol=1e-4 all sensors (not safe)	6.081020	6.656225	1.853271	4.421535	5.899599	19.748987	8.555593
dASIF dt=1 tol=1e-4 no sensors (safe)	8.719481	85.466763	1900.920043	2.619888	8.856243	60000.210210	8.787915
dASIF dt=1 tol=1e-4 no sensors (not safe)	8.403860	118.391181	1610.316620	2.576704	8.586583	32876.944156	3.994396
dASIF dt=10 tol=1e-4 all sensors (safe)	7.035054	7.514595	2.371262	4.521534	6.301900	20.624789	14.882400
dASIF dt=10 tol=1e-4 all sensors (not safe)	7.170553	7.600403	2.567077	4.440335	6.454838	62.132830	14.325055
dASIF dt=10 tol=1e-4 no sensors (safe)	12.820199	219.127918	2765.933881	2.769523	12.631502	60000.123889	12.427414
dASIF dt=10 tol=1e-4 no sensors (not safe)	11.966611	331.040660	3731.542520	2.683378	11.765680	60000.235233	15.292397
iASIF dt=1 all sensors (safe)	5.394485	5.523652	0.626012	4.872785	5.198343	9.845719	7.048852
iASIF dt=1 all sensors (not safe)	5.397487	5.534790	0.604243	4.909055	5.242497	8.479896	8.634139
iASIF dt=1 no sensors (safe)	5.216871	5.421575	0.551656	4.912907	5.103218	9.782077	6.681380
iASIF dt=1 no sensors (not safe)	5.578445	5.634629	0.593101	4.950629	5.461640	8.955738	9.248657
iASIF dt=10 all sensors (safe)	0.572849	0.588172	0.070050	0.524144	0.536647	0.948226	1.069346
iASIF dt=10 all sensors (not safe)	0.536340	0.560853	0.065782	0.523822	0.534903	1.224569	0.795307
iASIF dt=10 no sensors (safe)	0.547699	0.576585	0.057893	0.533684	0.545427	0.825248	0.799219
iASIF dt=10 no sensors (not safe)	0.590823	0.597209	0.066921	0.525249	0.548333	0.976318	0.819318

V. Discussion

This section discusses the main results and trends found while running experiments on each processor. The full results are presented in Section IV.

A. Commercial Off The Shelf NVIDIA Boards

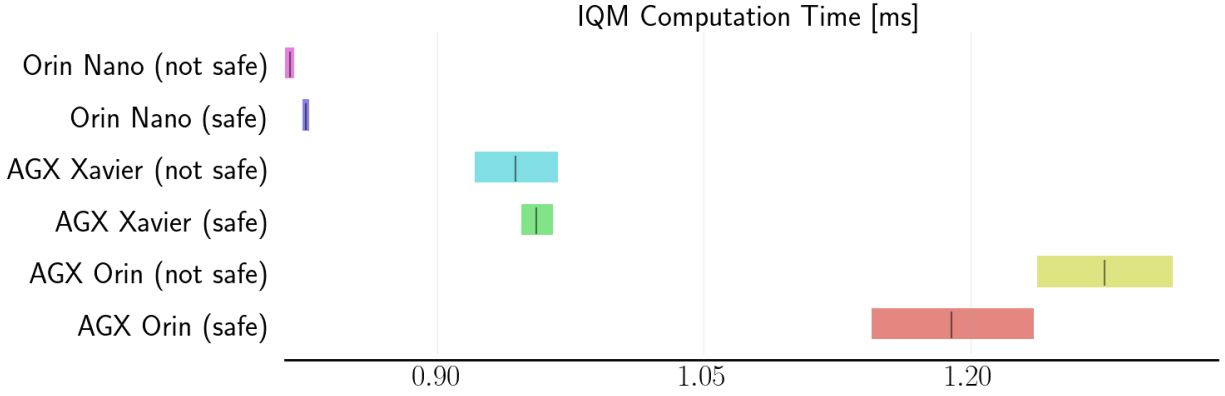


Fig. 4 NNC only (all sensors)

Fig. 4 shows the IQM of computation time for the NNC only across each COTS processor. The data shows that the Orin Nano is able to run the NNC the fastest, while the AGX Orin is the slowest. In this case, safe states and not safe states have very little difference on the computation time of the NNC. On any processor, the NNC is typically able to run in less than 1.5 ms, and Table 3 shows the MOET is 5.3 ms.

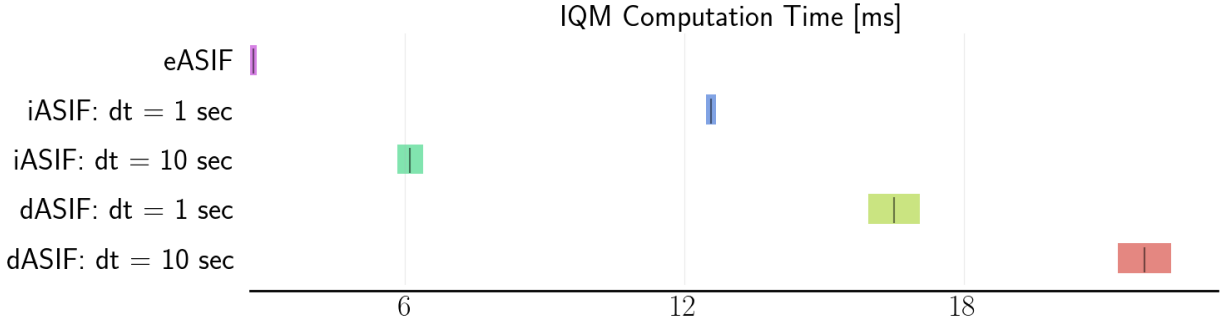


Fig. 5 RTA only - AGX Orin

Fig. 5 shows the computation time for each RTA configuration on the AGX Orin, all with safe states only. While only one processor is shown, the results show a similar trend found on the other processors. eASIF is shown to be the fastest configuration at less than 5 ms, which is intuitive as it requires the least computation to construct the barrier constraints. iASIF is the next fastest, where a 10 s timestep is faster than a 1 s timestep because it requires fewer trajectory states to be computed. dASIF is shown to be the slowest, notably because of the nonlinear solver. A 1 s timestep is faster than a 10 s timestep in this case because a state 1 s into the future is more likely to be safe than a state 10 s into the future, and safe states allow the nonlinear solver to find a safe solution faster. Table 4 shows that the MOET for eASIF, iASIF, and dASIF using safe states are 13.2, 27.6, and 173.4 ms respectively. The MOET for dASIF is clearly much slower, which again enforces that nonlinear solvers are incomplete and can cause long computation times. While eASIF and iASIF both have advantages to the designer, in most cases dASIF should only be used over eASIF if it cannot run fast enough in real time for continuous control.

Fig. 6 shows the computation time for eASIF on each processor. The data shows that the AGX Orin is the fastest in this case, while the AGX Xavier is the slowest. This trend is similar for all of the RTA configurations. These results

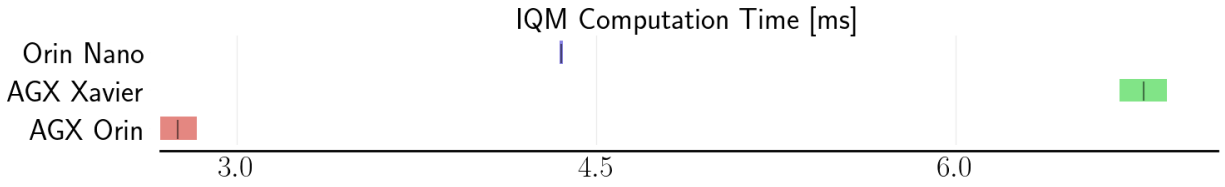


Fig. 6 RTA only (eASIF) - comparing processors

show that different processors provide different advantages for running the NNC or RTA.

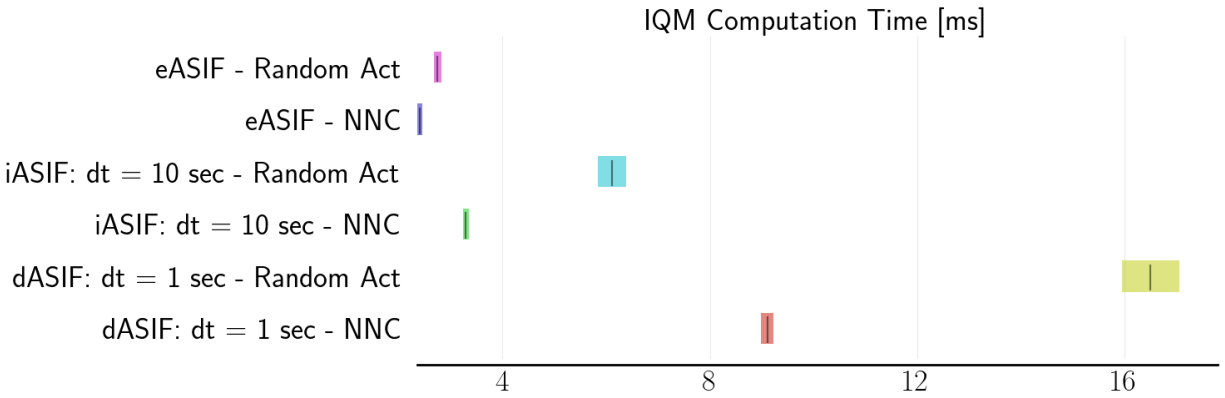


Fig. 7 RTA + NNC - AGX Orin

Finally, Fig. 7 shows the computation time for the NNC combined with RTA for the AGX Orin, compared to RTA only with random actions. The best performing RTA configurations are shown, but the trends are similar for all other configurations and processors. The data shows that for each RTA configuration, combining it with the NNC is faster than using random actions. This is because the NNC is more likely to produce safe actions, which allows the RTA to find a safe solution faster. This also shows that the computation time for the NNC combined with the RTA is not simply adding the computation time of the NNC only and RTA only, but rather the two systems can work together to reduce the total time.

B. Radiation Tolerant Unibap iX10

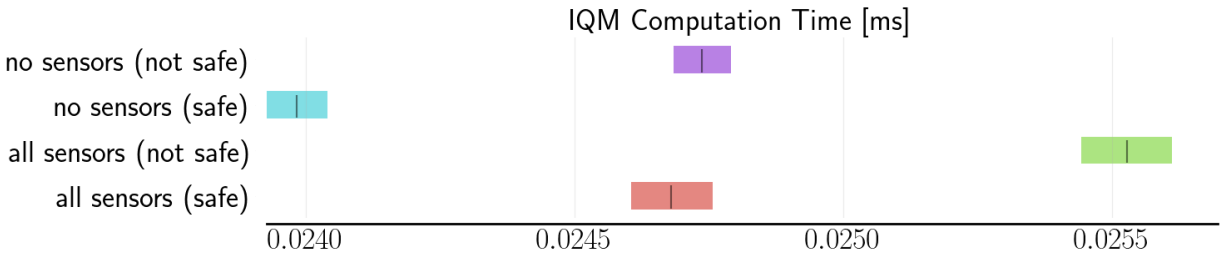


Fig. 8 NNC only

Fig. 8 shows the computation time for NNC only on the iX10. When comparing the two different NNCs, the data shows that the no sensors configuration is faster than the all sensors configuration because it has less model inputs and requires less computation. It can also be seen that safe states are faster than not safe states, because they are less likely to match the scenarios used to train the NNC. Overall, the NNC is typically able to run in less than 0.03 ms, and Table 6

shows the MOET is 0.16 ms.

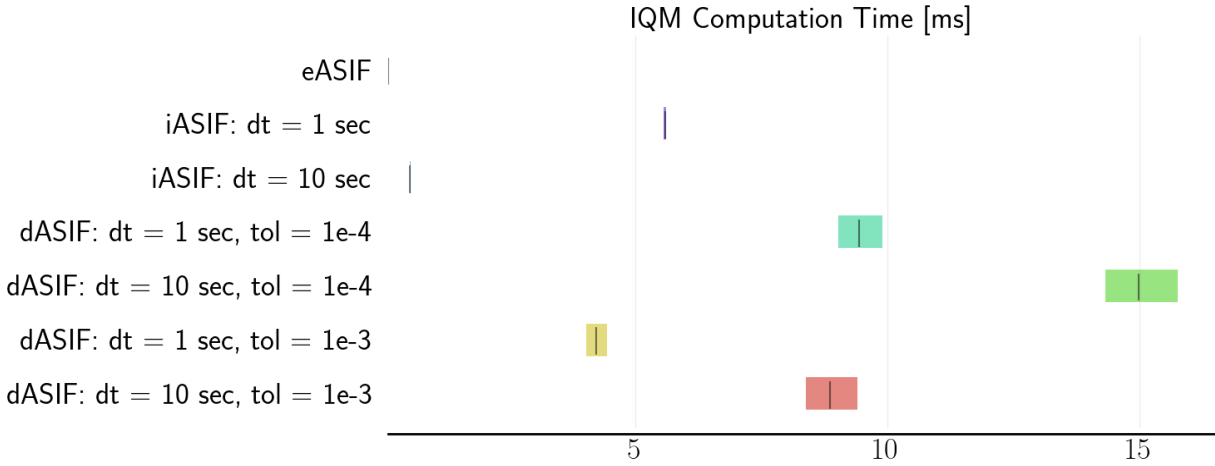


Fig. 9 RTA only

Fig. 9 shows the computation time for RTA only, with safe states only. The results follow the trends of Fig. 5, where eASIF is the fastest and dASIF is the slowest. For dASIF, having a smaller tolerance requires more time for the solver to find a solution because it must be more precise. Table 7 shows that the MOET for eASIF, iASIF, and dASIF using safe states are 0.40, 8.72, and 60,000 ms respectively, where the nonlinear solver was stopped at 60 s. Note that the dASIF times could be greatly reduced with further optimization to the nonlinear solver and potentially selecting a different algorithm to solve the problem.

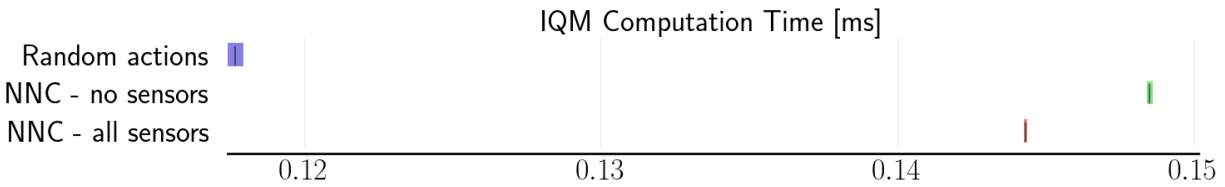


Fig. 10 NNC + eASIF

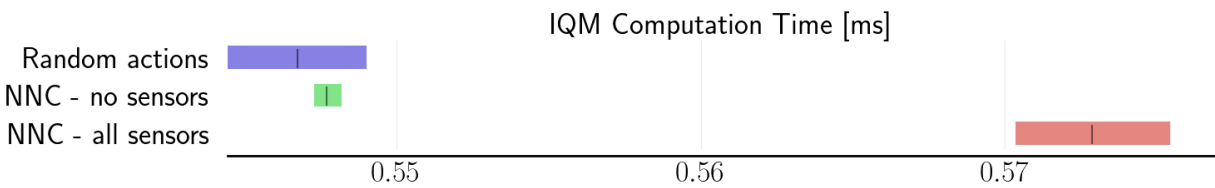


Fig. 11 NNC + iASIF: dt = 10

Fig. 10 shows the computation time for eASIF only compared to the NNC combined with eASIF, and Fig. 11 and Fig. 12 show the same comparison for the best performing iASIF and dASIF configurations respectively. For eASIF and iASIF, the data shows that using random actions is faster than combining the NNC and RTA because the computation time for matrix conversion outweighs the computation time for safer actions. However, for dASIF, safe actions are more impactful in lowering the computation time as they allow the nonlinear solver to compute the correct solution in fewer steps.

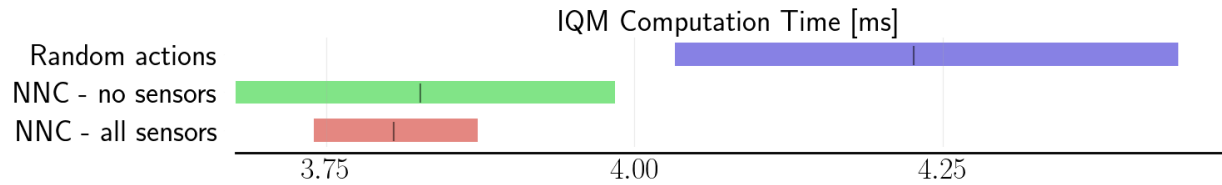


Fig. 12 NNC + dASIF: $dt = 1$, $tol = 1e-3$

VI. Conclusion

This paper presented many different experiments where an NNC and RTA filter were run on COTS and radiation tolerant processors. For the spacecraft inspection task defined in this paper, it is estimated that a control system consisting of an NNC and RTA filter would not need to run faster than 10 Hz in real time. Based on the MOET for each configuration tested, this can be achieved for all configurations on COTS and radiation tolerant processors except for dASIF. It is recommended that eASIF be used on any of these processors over dASIF since it has the ability to run in real time. However, the dASIF algorithm could be further optimized by adjusting solver parameters such as the algorithm used. In general, all algorithms tested in this paper should be further optimized before application to a real world platform. Importantly, it was found that using a primary controller that produces safe actions allows an RTA filter to solve the optimization problem faster. While many other algorithms and processes must be run on board space grade hardware, these results suggest that an NNC and RTA filter can be run in real time on board COTS and radiation tolerant processors. Future work will consist of repeating these experiments on radiation hardened processors.

Acknowledgments

This research was sponsored by the Air Force Research Laboratory under the *Safe Trusted Autonomy for Responsible Spacecraft* (STARS) Seedlings for Disruptive Capabilities Program. The views expressed are those of the authors and do not reflect the official guidance or position of the United States Government, the Department of Defense, or of the United States Air Force. This work has been approved for public release: distribution unlimited. Case Number AFRL-2024-2470.

References

- [1] Silver, D., Huang, A., Maddison, C., Guez, A., Sifre, L., Driessche, G., Schrittwieser, J., Antonoglou, I., Panneershelvam, V., Lanctot, M., Dieleman, S., Grewe, D., Nham, J., Kalchbrenner, N., Sutskever, I., Lillicrap, T., Leach, M., Kavukcuoglu, K., Graepel, T., and Hassabis, D., “Mastering the Game of Go with Deep Neural Networks and Tree Search,” *Nature*, Vol. 529, 2016, pp. 484–489. <https://doi.org/10.1038/nature16961>.
- [2] Vinyals, O., Babuschkin, I., Czarnecki, W. M., Mathieu, M., Dudzik, A., Chung, J., Choi, D. H., Powell, R., Ewalds, T., Georgiev, P., et al., “Grandmaster level in StarCraft II using multi-agent reinforcement learning,” *Nature*, Vol. 575, No. 7782, 2019, pp. 350–354.
- [3] Wurman, P. R., Barrett, S., Kawamoto, K., MacGlashan, J., Subramanian, K., Walsh, T. J., Capobianco, R., Devlic, A., Eckert, F., Fuchs, F., et al., “Outracing champion Gran Turismo drivers with deep reinforcement learning,” *Nature*, Vol. 602, No. 7896, 2022, pp. 223–228.
- [4] Ravaioli, U. J., Cunningham, J., McCarroll, J., Gangal, V., Dunlap, K., and Hobbs, K. L., “Safe Reinforcement Learning Benchmark Environments for Aerospace Control Systems,” *2022 IEEE Aerospace Conference (50100)*, IEEE, 2022, pp. 1–18.
- [5] Hamilton, N., Musau, P., Lopez, D. M., and Johnson, T. T., “Zero-Shot Policy Transfer in Autonomous Racing: Reinforcement Learning vs Imitation Learning,” *2022 IEEE International Conference on Assured Autonomy (ICAA, 2022)*, pp. 11–20. <https://doi.org/10.1109/ICAA52185.2022.00011>.
- [6] van Wijk, D., Dunlap, K., Majji, M., and Hobbs, K., “Deep Reinforcement Learning for Autonomous Spacecraft Inspection using Illumination,” *AAS/AIAA Astrodynamics Specialist Conference, Big Sky, Montana*, 2023.
- [7] Brandonisio, A., Lavagna, M., and Guzzetti, D., “Reinforcement learning for uncooperative space objects smart imaging path-planning,” *The Journal of the Astronautical Sciences*, Vol. 68, No. 4, 2021, pp. 1145–1169.

- [8] Oestreich, C. E., Linares, R., and Gondhalekar, R., “Autonomous six-degree-of-freedom spacecraft docking with rotating targets via reinforcement learning,” *Journal of Aerospace Information Systems*, Vol. 18, No. 7, 2021, pp. 417–428.
- [9] Broida, J., and Linares, R., “Spacecraft Rendezvous Guidance in Cluttered Environments via Reinforcement Learning,” *29th AAS/AIAA Space Flight Mechanics Meeting*, 2019, pp. 1–15.
- [10] Hovell, K., and Ulrich, S., “Deep reinforcement learning for spacecraft proximity operations guidance,” *Journal of spacecraft and rockets*, Vol. 58, No. 2, 2021, pp. 254–264.
- [11] Hamilton, N., Dunlap, K., Johnson, T. T., and Hobbs, K. L., “Ablation study of how run time assurance impacts the training and performance of reinforcement learning agents,” *2023 IEEE 9th International Conference on Space Mission Challenges for Information Technology (SMC-IT)*, IEEE, 2023, pp. 45–55.
- [12] Jang, K., Vinitzky, E., Chalaki, B., Remer, B., Beaver, L., Malikopoulos, A. A., and Bayen, A., “Simulation to scaled city: zero-shot policy transfer for traffic control via autonomous vehicles,” *Proceedings of the 10th ACM/IEEE International Conference on Cyber-Physical Systems*, 2019, pp. 291–300.
- [13] Kadian, A., Truong, J., Gokaslan, A., Clegg, A., Wijmans, E., Lee, S., Savva, M., Chernova, S., and Batra, D., “Are we making real progress in simulated environments? measuring the sim2real gap in embodied visual navigation,” *arXiv preprint arXiv:1912.06321*, 2019.
- [14] Alshiekh, M., Bloem, R., Ehlers, R., Könighofer, B., Niekum, S., and Topcu, U., “Safe reinforcement learning via shielding,” *Thirty-Second AAAI Conference on Artificial Intelligence*, 2018, pp. 2669–2678.
- [15] Fulton, N., and Platzer, A., “Safe reinforcement learning via formal methods,” *AAAI Conference on Artificial Intelligence*, 2018, p. 6485–6492.
- [16] Fisac, J. F., Akametalu, A. K., Zeilinger, M. N., Kaynama, S., Gillula, J., and Tomlin, C. J., “A general safety framework for learning-based control in uncertain robotic systems,” *IEEE Transactions on Automatic Control*, Vol. 64, No. 7, 2018, pp. 2737–2752.
- [17] Zhao, H., Zeng, X., Chen, T., Liu, Z., and Woodcock, J., “Learning Safe Neural Network Controllers with Barrier Certificates,” *International Symposium on Dependable Software Engineering: Theories, Tools, and Applications*, Springer, 2020, pp. 177–185.
- [18] Hunt, N., Fulton, N., Magliacane, S., Hoang, T. N., Das, S., and Solar-Lezama, A., “Verifiably Safe Exploration for End-to-End Reinforcement Learning,” *Proceedings of the 24th International Conference on Hybrid Systems: Computation and Control*, Association for Computing Machinery, New York, NY, USA, 2021, p. 1–11.
- [19] Li, Y., Li, N., Tseng, H. E., Girard, A., Filev, D., and Kolmanovsky, I., “Safe reinforcement learning using robust action governor,” *Learning for Dynamics and Control*, PMLR, 2021, pp. 1093–1104.
- [20] Zhang, L., Zhang, R., Wu, T., Weng, R., Han, M., and Zhao, Y., “Safe Reinforcement Learning With Stability Guarantee for Motion Planning of Autonomous Vehicles,” *IEEE Transactions on Neural Networks and Learning Systems*, 2021, pp. 1–10. <https://doi.org/10.1109/TNNLS.2021.3084685>.
- [21] Wagener, N. C., Boots, B., and Cheng, C.-A., “Safe reinforcement learning using advantage-based intervention,” *International Conference on Machine Learning*, PMLR, 2021, pp. 10630–10640.
- [22] Hamilton, N., Robinette, P., and Johnson, T., “Training Agents to Satisfy Timed and Untimed Signal Temporal Logic Specifications with Reinforcement Learning,” *Software Engineering and Formal Methods*, 2022.
- [23] Dunlap, K., Mote, M., Delsing, K., and Hobbs, K. L., “Run time assured reinforcement learning for safe satellite docking,” *Journal of Aerospace Information Systems*, Vol. 20, No. 1, 2023, pp. 25–36.
- [24] Hobbs, K. L., Mote, M. L., Abate, M. C., Coogan, S. D., and Feron, E. M., “Runtime assurance for safety-critical systems: An introduction to safety filtering approaches for complex control systems,” *IEEE Control Systems Magazine*, Vol. 43, No. 2, 2023, pp. 28–65.
- [25] Lovelly, T. M., and George, A. D., “Comparative analysis of present and future space-grade processors with device metrics,” *Journal of aerospace information systems*, Vol. 14, No. 3, 2017, pp. 184–197.
- [26] Dunlap, K., van Wijk, D., and Hobbs, K. L., “Run Time Assurance for Autonomous Spacecraft Inspection,” *2023 AAS/AIAA Astrodynamics Specialist Conference, Big Sky, MT*, 2023.

- [27] Hamilton, N., Schlemmer, L., Menart, C., Waddington, C., Jenkins, T., and Johnson, T. T., “Sonic to knuckles: evaluations on transfer reinforcement learning,” *Unmanned Systems Technology XXII*, Vol. 11425, International Society for Optics and Photonics, 2020, p. 114250J.
- [28] Brockman, G., Cheung, V., Pettersson, L., Schneider, J., Schulman, J., Tang, J., and Zaremba, W., “Openai gym,” *arXiv preprint arXiv:1606.01540*, 2016.
- [29] Henderson, P., Islam, R., Bachman, P., Pineau, J., Precup, D., and Meger, D., “Deep reinforcement learning that matters,” *Proceedings of the AAAI conference on artificial intelligence*, Vol. 32, 2018, pp. 3207–3214.
- [30] Mania, H., Guy, A., and Recht, B., “Simple random search of static linear policies is competitive for reinforcement learning,” *Proceedings of the 32nd International Conference on Neural Information Processing Systems*, 2018, pp. 1805–1814.
- [31] Bernini, N., Bessa, M., Delmas, R., Gold, A., Goubault, E., Pennek, R., Putot, S., and Sillion, F., “A few lessons learned in reinforcement learning for quadcopter attitude control,” *Proceedings of the 24th International Conference on Hybrid Systems: Computation and Control*, 2021, pp. 1–11.
- [32] Schulman, J., Wolski, F., Dhariwal, P., Radford, A., and Klimov, O., “Proximal policy optimization algorithms,” *arXiv preprint arXiv:1707.06347*, 2017.
- [33] Nagumo, M., “Über die lage der integralkurven gewöhnlicher differentialgleichungen,” *Proceedings of the Physico-Mathematical Society of Japan. 3rd Series*, Vol. 24, 1942, pp. 551–559.
- [34] Ames, A. D., Coogan, S., Egerstedt, M., Notomista, G., Sreenath, K., and Tabuada, P., “Control barrier functions: Theory and applications,” *2019 18th European control conference (ECC)*, IEEE, 2019, pp. 3420–3431.
- [35] Gurriet, T., Singletary, A., Reher, J., Ciarletta, L., Feron, E., and Ames, A., “Towards a Framework for Realizable Safety Critical Control through Active Set Invariance,” *2018 ACM/IEEE 9th International Conference on Cyber-Physical Systems (ICCPS)*, 2018, pp. 98–106. <https://doi.org/10.1109/ICCPS.2018.00018>.
- [36] Chen, Y., Jankovic, M., Santillo, M., and Ames, A. D., “Backup control barrier functions: Formulation and comparative study,” *2021 60th IEEE Conference on Decision and Control (CDC)*, IEEE, 2021, pp. 6835–6841.
- [37] Xiong, Y., Zhai, D.-H., Tavakoli, M., and Xia, Y., “Discrete-Time Control Barrier Function: High-Order Case and Adaptive Case,” *IEEE Transactions on Cybernetics*, Vol. 53, No. 5, 2023, pp. 3231–3239. <https://doi.org/10.1109/TCYB.2022.3170607>.
- [38] Hill, G. W., “Researches in the Lunar Theory,” *American journal of Mathematics*, Vol. 1, No. 1, 1878, pp. 5–26.
- [39] Clohessy, W., and Wiltshire, R., “Terminal Guidance System for Satellite Rendezvous,” *Journal of the Aerospace Sciences*, Vol. 27, No. 9, 1960, pp. 653–658.
- [40] Merrick, J. D., Heiner, B. K., Long, C., Stieber, B., Fierro, S., Gangal, V., Blake, M., and Blackburn, J., “CoRL: Environment Creation and Management Focused on System Integration,” , 2023. <https://doi.org/https://doi.org/10.48550/arXiv.2303.02182>.
- [41] Ravaioli, U. J., Dunlap, K., and Hobbs, K., “A Universal Framework for Generalized Run Time Assurance with JAX Automatic Differentiation,” *2023 American Control Conference (ACC)*, 2023, pp. 4264–4269. <https://doi.org/10.23919/ACC55779.2023.10156439>.
- [42] “ONNX Runtime,” <https://onnxruntime.ai/>, 2021.
- [43] “quadprog,” <https://github.com/quadprog/quadprog>, 2024.
- [44] Virtanen, P., Gommers, R., Oliphant, T. E., Haberland, M., Reddy, T., Cournapeau, D., Burovski, E., Peterson, P., Weckesser, W., Bright, J., van der Walt, S. J., Brett, M., Wilson, J., Millman, K. J., Mayorov, N., Nelson, A. R. J., Jones, E., Kern, R., Larson, E., Carey, C. J., Polat, İ., Feng, Y., Moore, E. W., VanderPlas, J., Laxalde, D., Perktold, J., Cimrman, R., Henriksen, I., Quintero, E. A., Harris, C. R., Archibald, A. M., Ribeiro, A. H., Pedregosa, F., van Mulbregt, P., and SciPy 1.0 Contributors, “SciPy 1.0: Fundamental Algorithms for Scientific Computing in Python,” *Nature Methods*, Vol. 17, 2020, pp. 261–272. <https://doi.org/10.1038/s41592-019-0686-2>.
- [45] Harris, C. R., Millman, K. J., van der Walt, S. J., Gommers, R., Virtanen, P., Cournapeau, D., Wieser, E., Taylor, J., Berg, S., Smith, N. J., Kern, R., Picus, M., Hoyer, S., van Kerkwijk, M. H., Brett, M., Haldane, A., del Río, J. F., Wiebe, M., Peterson, P., Gérard-Marchant, P., Sheppard, K., Reddy, T., Weckesser, W., Abbasi, H., Gohlke, C., and Oliphant, T. E., “Array programming with NumPy,” *Nature*, Vol. 585, No. 7825, 2020, pp. 357–362. <https://doi.org/10.1038/s41586-020-2649-2>, URL <https://doi.org/10.1038/s41586-020-2649-2>.

- [46] Macenski, S., Foote, T., Gerkey, B., Lalancette, C., and Woodall, W., “Robot Operating System 2: Design, architecture, and uses in the wild,” *Science Robotics*, Vol. 7, No. 66, 2022, p. eabm6074. <https://doi.org/10.1126/scirobotics.abm6074>, URL <https://www.science.org/doi/abs/10.1126/scirobotics.abm6074>.
- [47] “QuadProg++,” <https://github.com/liuq/QuadProgpp>, 2024.
- [48] Johnson, S. G., “The NLOpt nonlinear-optimization package,” <https://github.com/stevengj/nlopt>, 2007.
- [49] Guennebaud, G., Jacob, B., et al., “Eigen v3,” <http://eigen.tuxfamily.org>, 2010.
- [50] Agarwal, R., Schwarzer, M., Castro, P. S., Courville, A. C., and Bellemare, M., “Deep reinforcement learning at the edge of the statistical precipice,” *Advances in Neural Information Processing Systems*, Vol. 34, 2021.
- [51] Wilhelm, R., Engblom, J., Ermedahl, A., Holsti, N., Thesing, S., Whalley, D., Bernat, G., Ferdinand, C., Heckmann, R., Mitra, T., et al., “The worst-case execution-time problem—overview of methods and survey of tools,” *ACM Transactions on Embedded Computing Systems (TECS)*, Vol. 7, No. 3, 2008, pp. 1–53.